



# Modification of grain refinement and texture based on pre-upsetting AZ31 Mg alloy in interactive alternating forward extrusion

Hua Qiu Du<sup>1</sup> · Feng Li<sup>1,2</sup> · Ye Wang<sup>1</sup> · Chao Li<sup>1</sup> · Zi Yu Chen<sup>1</sup>

Received: 19 January 2022 / Accepted: 2 July 2022 / Published online: 11 July 2022  
© The Author(s), under exclusive licence to Springer-Verlag London Ltd., part of Springer Nature 2022

## Abstract

Reducing energy consumption and exploring the potential of materials in depth is a long-term pursuit of goals and development directions in the field of extrusion technology. If load reduction and material performance can be achieved at the same time, this is a good strategy to solve the bottleneck. For the first time, a pre-upsetting technique was used before alternating extrusion in this investigation, which enhances grain refinement and increases the Schmid factor. This reduced the single grain yield strength and the load of the second process. The results of comparative research show that compared with interactive alternating forward extrusion (AFE), pre-upsetting alternate forward extrusion (UAFE) can significantly reduce the peak load required for forming, which increases the tensile strength of extruded AZ31 magnesium alloy products by 41.9% and the ductility to 23.7%. The average grain size was only 1/2 of the conventional alternating extrusion grain size, and the strength of the texture was weakened to 8.62. The increase in tensile strength is mainly due to fine-grained strengthening. Grain boundaries can hinder dislocation movement. Some grains are inclined from the original typical fiber texture to the ED direction during pre-upsetting, which effectively reduces the texture strength of UAFE and increases the ductility of the material. This provides scientific guidance and technical support for the development and application of high-performance magnesium alloy extrusion forming technology.

**Keywords** Magnesium alloy · Pre-upsetting · Alternate extrusion · Texture · Tensile strength · Ductility

## 1 Introduction

In recent years, because of their high comprehensive qualities, magnesium alloys have been thought to have considerable application prospects in aircraft, transportation, and other industries. [1–5]. However, magnesium alloys have a hexagonal close-packed (HCP) structure with a shortage of independent slip systems, which cannot meet the von Mises yield criterion [6]. This causes a bigger texture

to emerge during thermomechanical processing, reducing its ductility and formability at room temperature. Agnew et al. [7] made a great contribution to the weakening of magnesium alloy texture and proved that the weakening of the texture can further improve the product performance. Pan et al. [8] proposed a compound extrusion method in which magnesium alloy ingots are divided and rebound together. Compared with the traditional extrusion method, composite extrusion increases the ductility of magnesium alloy sheets from 18.5 to 22.5%, and the tensile strength is also correspondingly improved. This opens up a new avenue for the production of high-performance magnesium alloys. Lu et al. [9] designed a novel severe plastic deformation technique by integrating forward extrusion and torsion deformation into a single processing step and tested its feasibility for the Mg alloy AZ31. The grain size was reduced significantly from 300 to 3.5  $\mu\text{m}$ , and the strong basal texture formed in the forward extrusion can be further weakened. The fracture strain of the magnesium alloy bars is increased from 21 to 29%. Jiang et al. [10] developed an asymmetric extrusion (AE) process,

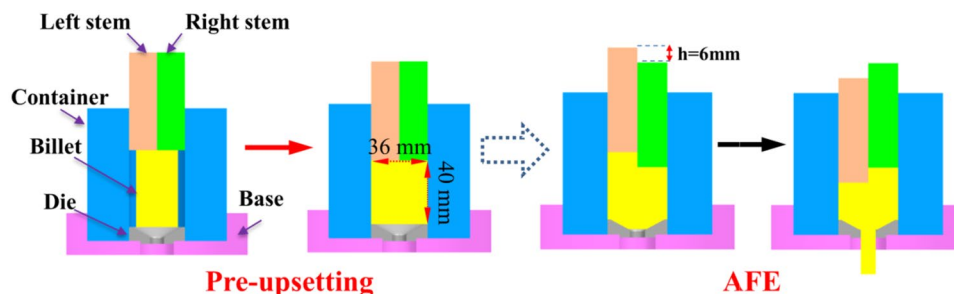
✉ Feng Li  
fli@hrbust.edu.cn

✉ Ye Wang  
wangye\_2017@126.com

<sup>1</sup> School of Materials Science and Chemical Engineering, Harbin University of Science and Technology, Harbin 150040, People's Republic of China

<sup>2</sup> Key Laboratory of Advanced Manufacturing and Intelligent Technology, Ministry of Education, Harbin University of Science and Technology, Harbin 150080, People's Republic of China

Fig. 1 Principle of UAFE



which provides an asymmetric shear strain during extrusion and thus introduces an effective strain gradient throughout the thickness of the sheets. Compared with the conventional extrusion AZ31 sheet, finer microstructures and weaker tilted basal textures were obtained in the AE AZ31 sheet. The ductility of the normal magnesium alloy extruded sheet increased from 19.1 to 27.3%. Li et al. [11] employed a continuous variable cross-section direct extrusion method to prepare high-performance magnesium alloys. By increasing the number of intermediate temporary molds, a variable cross-section is formed. Under the direct extrusion of the third-order continuous variable cross-section, the texture strength is greatly weakened compared with conventional extrusion. The tensile strength of the magnesium alloy bars increased from 251 to 291 MPa, and the ductility increased from 7.8 to 19.8%. Zhang et al. [12] studied the microstructure evolution and mechanical properties of AZ31 magnesium alloy sheets prepared by low-speed extrusion at different temperatures. A strong (0002) basal texture was observed within the prepared sheets, and the maximum basal texture intensity was reduced as the extrusion temperature rose. When the extrusion temperature was 623 K, the highest overall mechanical properties were observed, where the yield strength, tensile strength, and ductility were ~226 MPa, ~353 MPa, and ~16.7%, respectively.

The interactive alternating forward extrusion (AFE) process is a new method proposed in recent years and has received extensive attention from the industry [13, 14]. Instead of the typical overall structure, this method alternates downward loading and formation using two or more split stems. According to the difference in the loading mode of the split stem, it can be divided into two types: stepping and interactive. Compared with the stepping type, the interactive alternating extrusion method is more efficient. Interactive alternating extrusion was used in this paper. To

further realize labor-saving load reduction [15–18] and fine grain modification, a pre-upsetting process was added, which has an important influence on the structure and performance of the products after alternate extrusion.

## 2 Experimental

### 2.1 Technical principle

The textural strength of the initial billet can be reduced by predeformation [19], refining the grains and improving the formability of the material. As a result, this article tries to pre-upset the billet before alternate extrusion by selecting a billet that is smaller than the extrusion cylinder's inner diameter and placing it on the die. The center of the billet coincides with the extrusion axis. The two-part stems are first loaded synchronously downward, that is, pre-upsetting deformation so that the billet is compressed and deformed to fill the entire cavity. Then, the two split stems are loaded downward in an interactive manner until the billet is completely extruded into shape. The principle of UAFE is shown in Fig. 1.

### 2.2 Materials and process

The research used commercial extruded AZ31 magnesium alloy, and its chemical composition is shown in Table 1. The inner diameter of the extrusion cylinder was  $\Phi 40$  mm, and two specifications of cylinder billets were selected to facilitate comparison: one was a  $\Phi 36$  mm  $\times$  40 mm cylinder for UAFE, and the other was  $\Phi 40$  mm  $\times$  32 mm for conventional alternate extrusion. Before the experiment, the billets needed to be homogenized. It was kept in a 673 K box-type holding furnace for 12 h,

**Table 1** Chemical composition of AZ31 magnesium alloy (wt.%)

| Al   | Zn   | Mn   | Fe     | Si    | Cu     | Ni      | Mg  |
|------|------|------|--------|-------|--------|---------|-----|
| 3.20 | 0.86 | 0.36 | 0.0018 | 0.021 | 0.0022 | 0.00056 | Bal |

and a thermocouple was used to monitor the temperature in real time to ensure that the temperature fluctuated within 1 K. The extrusion work was carried out on the YT32-100 press produced by the Tianjin Forging Machine Tool Plant. Graphite was used as the lubricant, the forming temperature was 623 K, the extrusion speed was 1 mm/s, and the extrusion ratio was 15.68.

In this study, the pre-upsetting deformation was 8 mm. During the alternate extrusion molding process, the downward loading of the split stem was  $h = 6$  mm. The pre-upsetting component near the center and the edge of the die was used to cut out a cuboid sample of 7 mm × 4 mm × 3 mm. The observation samples of the same size are intercepted at the same position of the two formed products for metallographic structure observation and electron backscattering diffraction (EBSD). The scanning area of EBSD was 300  $\mu\text{m}$  × 300  $\mu\text{m}$ , the step length was 1.5  $\mu\text{m}$ , and channel 5 was used to analyze the obtained data.

The sample was ground on sandpaper and a machine-glazed finish. When the surface of the sample was mirrored, corrosion was carried out. A Leica metallurgical microscope was used to observe and analyze the microstructure. The sample was then electrolytically polished after being reground. The polishing liquid was a mixed solution of phosphoric acid and alcohol (volume ratio: 3:5). Polishing at 0.3 A electric current for 60 s, followed by 0.2 A electric current polishing for 60 s.

To compare the mechanical properties of extruded products under different conditions, a tensile performance test was performed on an Instron 5569 testing machine. The size of the test piece was  $\Phi 5$  mm × 50 mm, and the loading speed was 1 mm/min. An Apreo field-emission scanning electron microscope was used to observe and analyze the tensile fracture morphology. In addition to providing data for performance research, the fracture form and morphological characteristics of samples under

corresponding conditions can also be studied, which is crucial for identifying the fracture mechanism.

## 3 Results

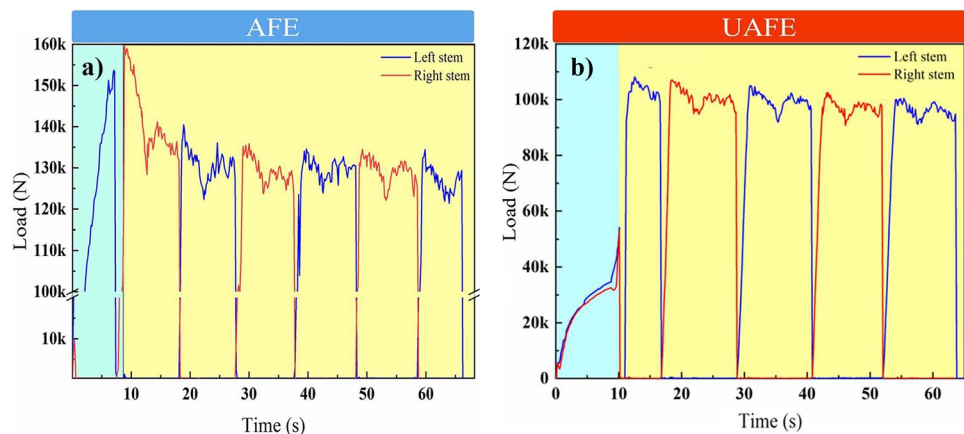
### 3.1 Extrusion load analysis

The extrusion process can be roughly divided into the filling extrusion stage, basic extrusion stage, and extrusion end stage. The load of the filling extrusion stage and the basic extrusion stage is investigated in this work, and the data were plotted in Figure 2 by Origin. The load-time line chart shows the first two stages. Refer to as UAFE and AFE as depicted in Figure 2. In these two stages, the load required for UAFE was much smaller than that required for AFE. The peak load of UAFE only needs 115 kN, while the peak load of alternate extrusion products reaches 159 kN. UAFE is very beneficial for saving labor, reducing load, and improving die life.

### 3.2 Microstructure evolution

The grain morphology comparison of alternate extrusion forming of magnesium alloy with and without pre-upsetting treatment is shown in Fig. 3. Figure 3a reveals that the initial extruded billet had a larger average grain size, with a particle size of 55–73  $\mu\text{m}$ . The metallographic structure of AFE is shown in Fig. 3b, and the grain refinement was obvious and relatively uniform (conjunction with Fig. 3e). The average particle size was approximately 10.05  $\mu\text{m}$ . The metallographic morphology of the UAFE is shown in Fig. 3c. In conjunction with Fig. 3f, it can be seen that the average particle size was only approximately 5.65  $\mu\text{m}$ . Figure 3d shows the stress state and the grain morphology at typical positions after pre-upsetting. The grains of the billet in the pre-upsetting stage have been refined to different degrees. In the middle area of the blue rectangle, coarser grains occupy the main position. At the same time, jagged grain boundaries

**Fig. 2** Experimental load comparison; **a** AFE and **b** UAFE



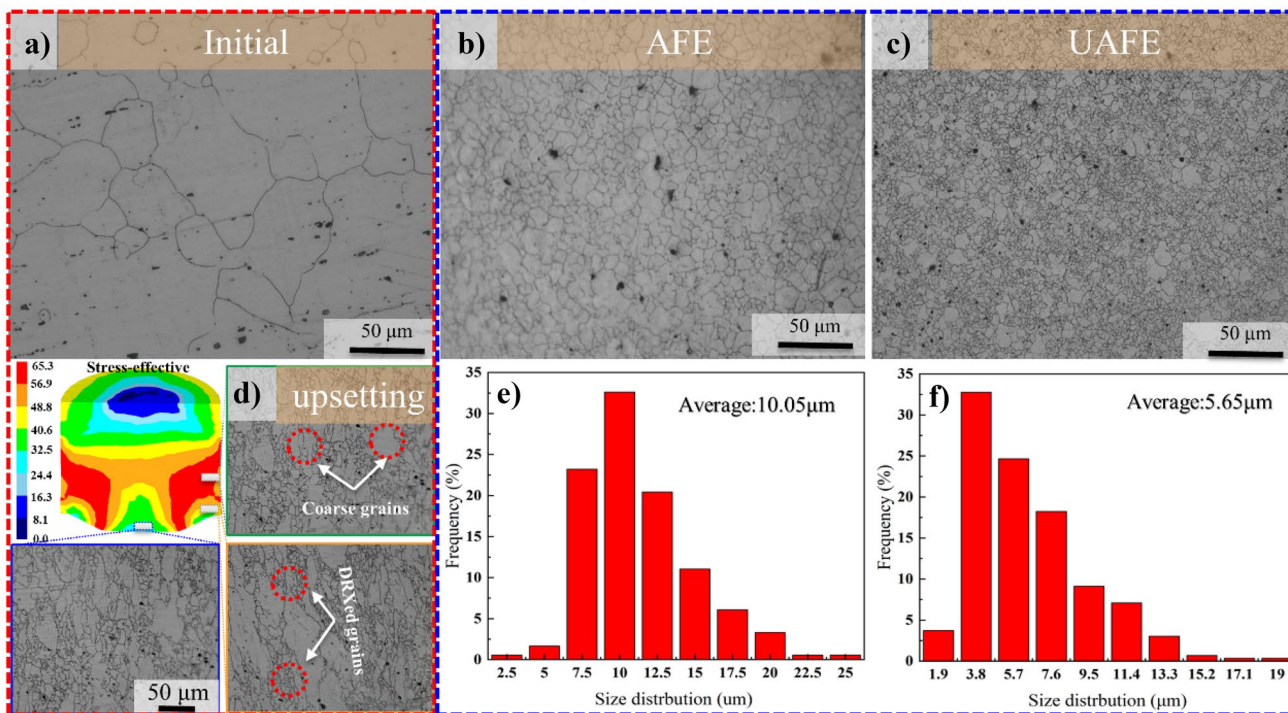


**Fig. 3** Optical micrographs obtained from the ED-ND plane of the products: **a** initial, **b** AFE, **c** UAFE, **d** micrographs after upsetting and internal effective strain, **e** grain size of AFE, and **f** grain size of UAFE

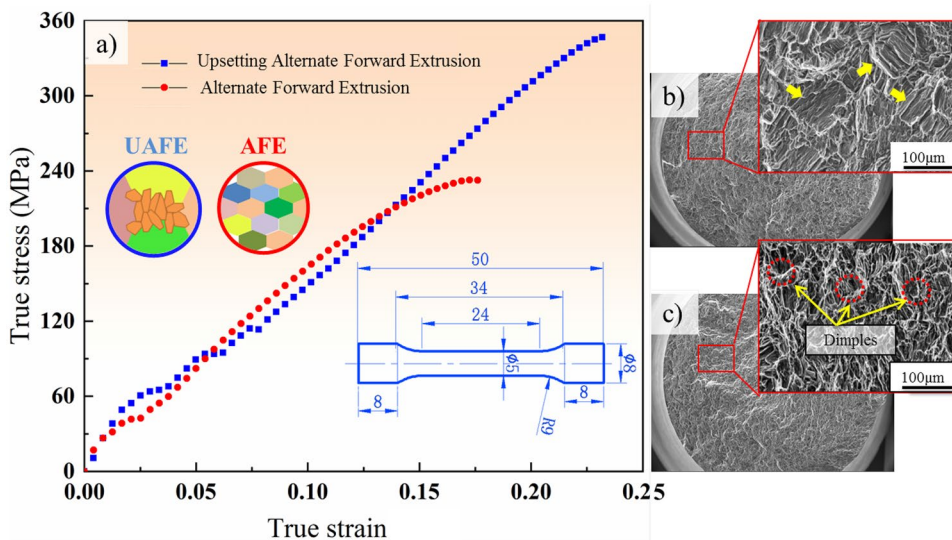
can be observed around the coarse grains, which may be the part where the recrystallized grains expand and nucleate through the grain boundaries [20].

The existing research results show that the particle size of AZ31 magnesium alloy alternating extrusion products is mostly in the range of 7.5 ~ 10.5 μm [21]. The grains obtained by alternate extrusion under the same conditions after the pre-upsetting treatment are smaller, and the grain sizes are mostly concentrated in the range of 3.2 ~ 5.8 μm.

### 3.3 Mechanical property

Figure 4 shows a comparison of the magnesium alloy’s tensile characteristics at room temperature. The upper left of the figure shows a schematic diagram of the internal grain morphology of the obtained product, and the lower right shows the actual size of the tensile sample. There were significant differences in the performance of the two molded products. The performance of UAFE is significantly better than that of

**Fig. 4** True stress-true strain curves of the products during tensile tests. **a** True stress-true strain curves, **b** AFE sample, and **c** UAFE sample



AFE. The tensile strength of the latter may reach 281 MPa, but the former can only reach 198 MPa, indicating a nearly 41.9% increase in strength. The ductility rate of conventional alternate extrusion is 12.5%, and alternately extruded products after pre-upsetting deformation can reach 23.7%, which is almost twice as high as the former.

Figures 4b and c show the fracture morphology of the two products after tensile testing at room temperature, and obvious necking can be observed. Conventional alternating extrusion products have large areas of cleavage steps, and a typical cleavage length is in excess of 50  $\mu\text{m}$ . The cleavage planes are inclined to the tensile axis at an angle very close to 45°, which corresponds to the inclination angle of the maximum shear stress planes in tension [22]. This fracture pattern is very common for deformation in magnesium alloys at low temperatures [23]. However, randomly distributed isometric dimples can be seen in the pre-upsetting alternately extruded products. This shows that the product has a relatively good plastic deformation ability, which can be mutually verified with the tensile performance.

The average grain size of the pre-upsetting alternately extruded products is small, only 5.65  $\mu\text{m}$ . A large number of subgrain boundaries were stored in the billet during the upsetting process. As the alternate extrusion loading process progresses, the subgrain boundaries gradually transform into high-angle grain boundaries [24], which play a role in grain refinement to a certain extent. According to the Hall–Petch relation ( $\sigma = \sigma_0 + kd^{-1/2}$ ) [25, 26], when the sample was subjected to tensile stress, it was evenly distributed to each fine grain. The greater the number of grains, the smaller the stress on each grain, and the greater the tensile stress it can

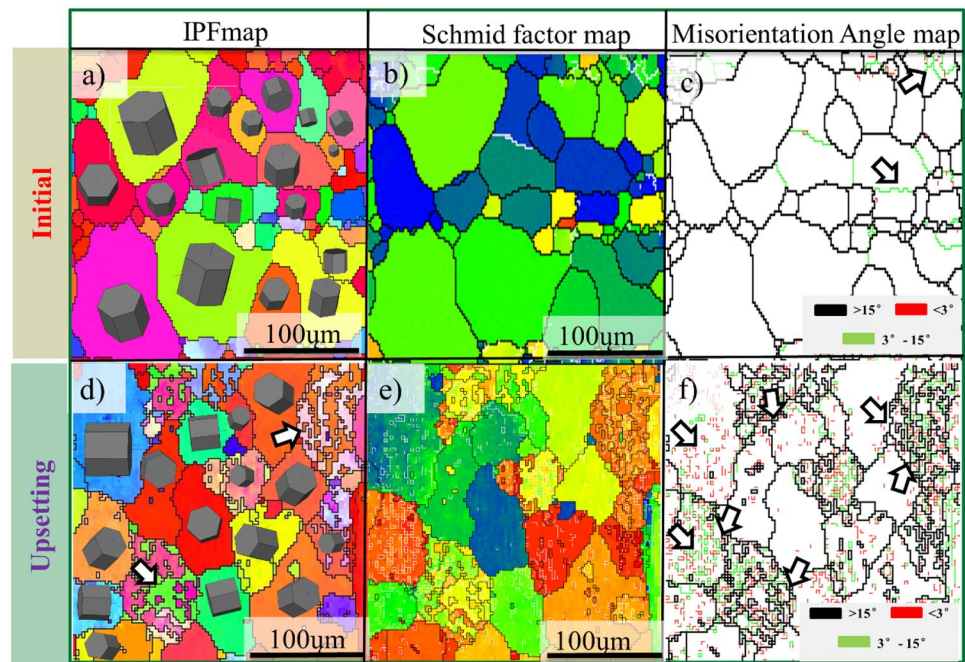
withstand [27]. Actually, there exists an intrinsic contradiction between the strength and ductility of metallic materials, which is related to the ability of dislocation motion. Grain refinement can effectively improve the yield strength of Mg alloys at the cost of sacrificial ductility [28]. In this study, due to material and process conditions, other strengthening mechanisms have weaker effects on strength, and grain refinement is more obvious. Therefore, the increase in strength is mainly attributed to the strengthening effect of fine grains. However, more research into the distorted microstructure is required to increase ductility.

## 4 Discussion

### 4.1 Schmid factor evolution

It can be seen from the above that the pre-upsetting alternating extrusion load of magnesium alloy is less than that of conventional alternating extrusion. Figures 5 and 6 show the statistics of the Schmid factor and grain boundary angle of the initial billet and pre-upsetting billet. Slip is the main deformation mode of magnesium alloys at high temperatures, which is essentially the movement of dislocations [29]. According to different slip planes, it can be divided into base slip, prismatic slip, and pyramidal slip. According to different slip directions, it can be divided into  $\langle a \rangle$  slip and  $\langle c + a \rangle$  slip. The basal and prismatic slips are unit dislocation slips with a Burgers vector of  $a/3 \langle 11\bar{2}0 \rangle$ . The Schmid factor is an important parameter that determines the slip of magnesium alloys.  $\tau_K = \sigma_s$

**Fig. 5** Schmid factors for basal slip, IPF, grain boundary structure distribution diagram of initial and upsetting (a, b, c) initial sample (d, e, f) upsetting sample



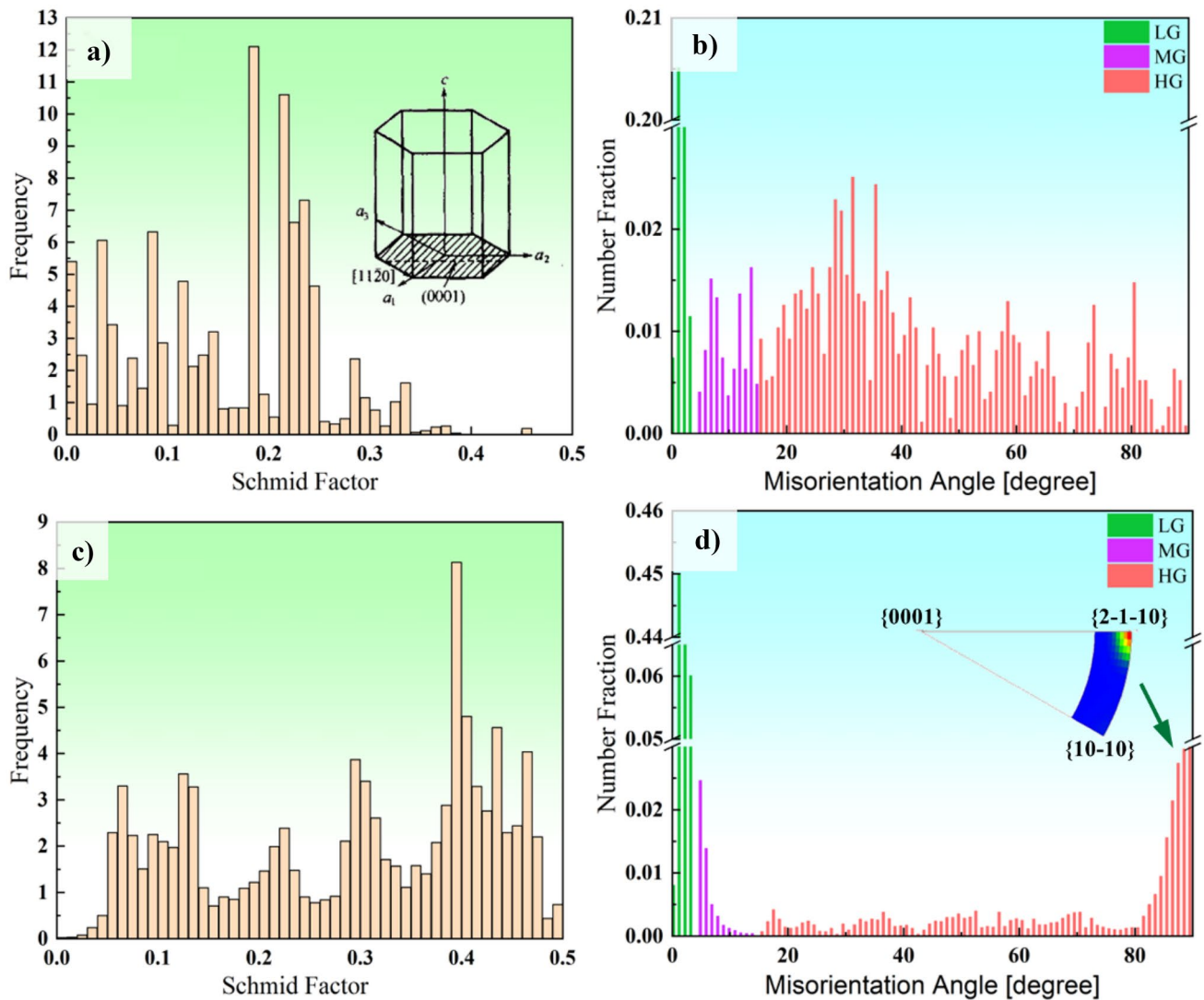


**Fig. 6** Schmid factor and misorientation angle distributions of the alloy under different conditions. **a, b** Initial sample; **a, d** upsetting sample

•  $\cos\phi \cdot \cos\lambda$ ,  $\cos\phi \cdot \cos\lambda$  was called the Schmid factor. When the crystal is under force, not all slip systems are activated at the same time but are determined by the force state [30]. Whether the slip system in the crystal starts depends on the force (axial tension) in the slip direction in the slip plane  $\tau$  (resolved shear stress) value [31]. The larger the Schmid factor is,  $\sigma_s$  will be smaller,  $\tau$  easily reaches the critical resolved shear stress (CRSS), and slip occurs, which causes multigrain slip and leads to macroscopic plastic deformation of the material [32]. In Fig. 5c, the number of red and yellow grains is large, and the rainbow color from red to blue represents the value of the Schmidt factor from high to low. It can be seen from the histogram of Fig. 6a and c that there are few grains with SF values exceeding 0.3 in the initial billet. After pre-upsetting deformation, the grains with SF values

exceeding 0.3 increase significantly, which indicates that the base plane Schmid factor is high and that the base slip easily starts.

In Fig. 5c and f and Fig. 6b and d, three kinds of grain boundaries (low-angle grain boundaries, grain boundary misorientation angle  $\theta_{GB} < 3^\circ$ ; high-angle grain boundaries,  $\theta_{GB} > 15^\circ$ ; medium angle grain boundaries, grain boundary misorientation angle,  $3^\circ < \theta_{GB} < 15^\circ$ ) [33] of pre-upsetting and initial billet are shown. In the histogram, blue represents the low-angle grain boundaries, green represents the medium-angle grain boundaries in the transition stage, and red represents the high-angle grain boundaries. It can be seen in the graph that the low-angle grain boundaries are densely distributed inside the billet after pre-upsetting, and the low-angle subgrain boundaries are usually caused by the accumulation of dislocations [34]. Studies have shown that

when grains are connected by a boundary with an orientation angle of less than 30°, basal slip is likely to start up [35]. In Fig. 6d, the orientation difference angle of 84~88° in the billet after pre-upsetting increases greatly, which may be related to the formation of tensile twins during the deformation of pre-upsetting. The orientation relationship between tensile twins and the matrix is  $86^\circ < 11\text{--}20 >$  [36].

By the statistical analysis of the Schmid factor and grain boundary angle, it can be preliminarily judged that the light load in the process of UAFE is caused by the easy start of the slip system in the upsetting state and the coordinated deformation of some refined grains.

### 4.2 Texture evolution during UAFE

The mechanical properties and deformation behavior of metal materials are dominated by their lattice structure [37, 38]. The properties of polycrystalline magnesium alloys are highly related to the grain arrangement and are not just a superposition of the properties of a single grain.

Figure 7 shows the pole figure and grain type statistics of AFE and UAFE. Figure 7a is an IPF map of the product by pre-upsetting alternately extruded. The basal planes of grains are almost parallel to the extrusion direction. The texture strength is almost zero in the RD direction. However, the internal grains of conventional alternating extrusion products mostly deflect in the ND direction. In Fig. 7a and b, it can also be observed that the maximum pole density of the pole figure is 8.62 and 12.92, respectively, and there is a significant difference in texture strength between the two products. The strength of the texture can affect the properties of metal products [39], and the basal-random GBs in UAFE texture samples hinder the transfer of basal slip and contribute to the activation of nonbasal slips [40]. To deeply study the causes of the texture of the two products, the regions with high pole density in the two pole figures are formed into subsets in channel 5 software to explore the composition of grain types. In Fig. 7e, the proportion of recrystallized grains reaches 45%, followed by deformed grains, and the minimum number of subgrains is only 17%. In Fig. 7b, the

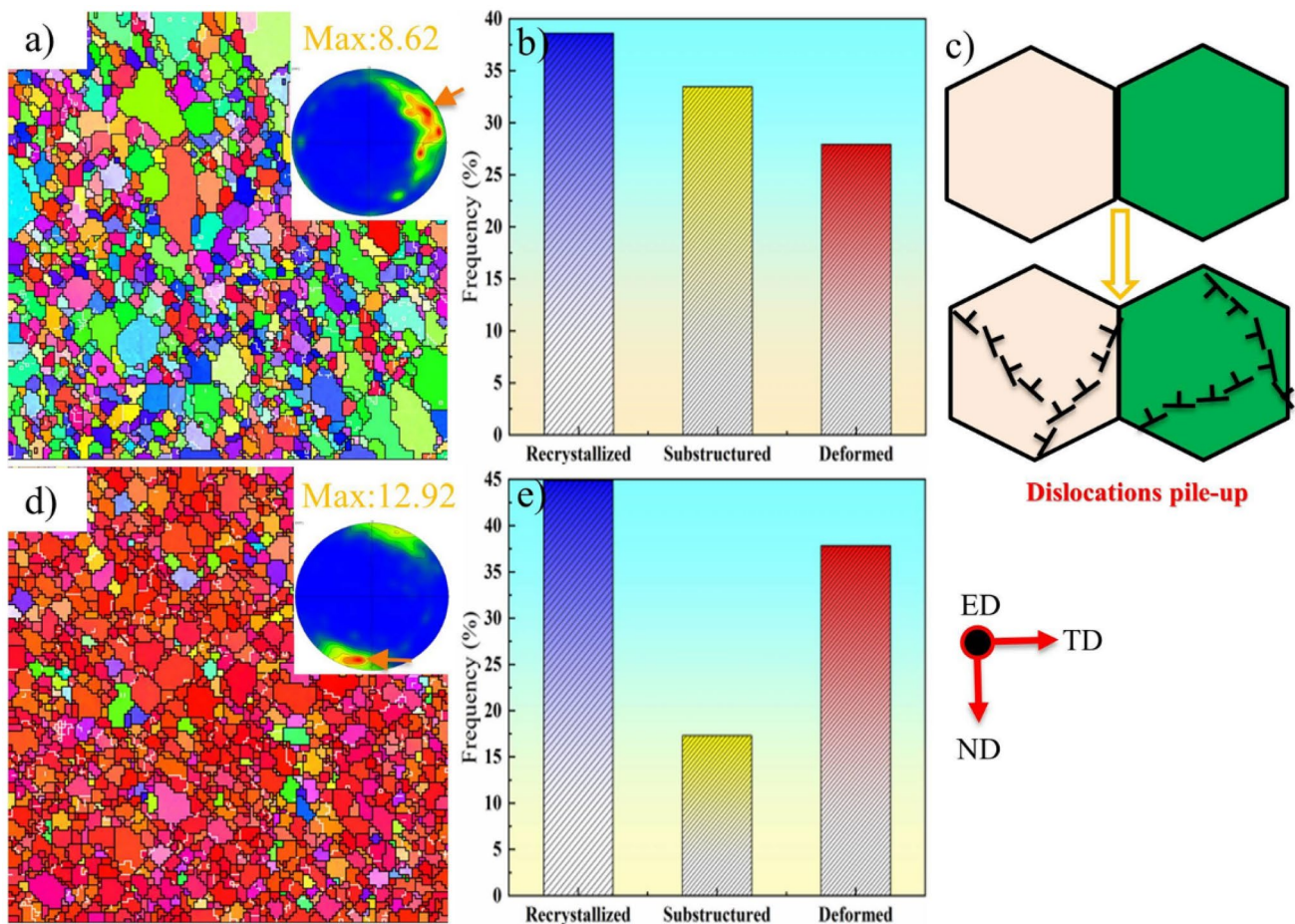


**Fig. 7** IPF maps and different grain types in the microstructure of samples: **a, b** UAFE sample; **c** schematic diagram s of CDRX of Mg alloys; and **d, e** AFE sample

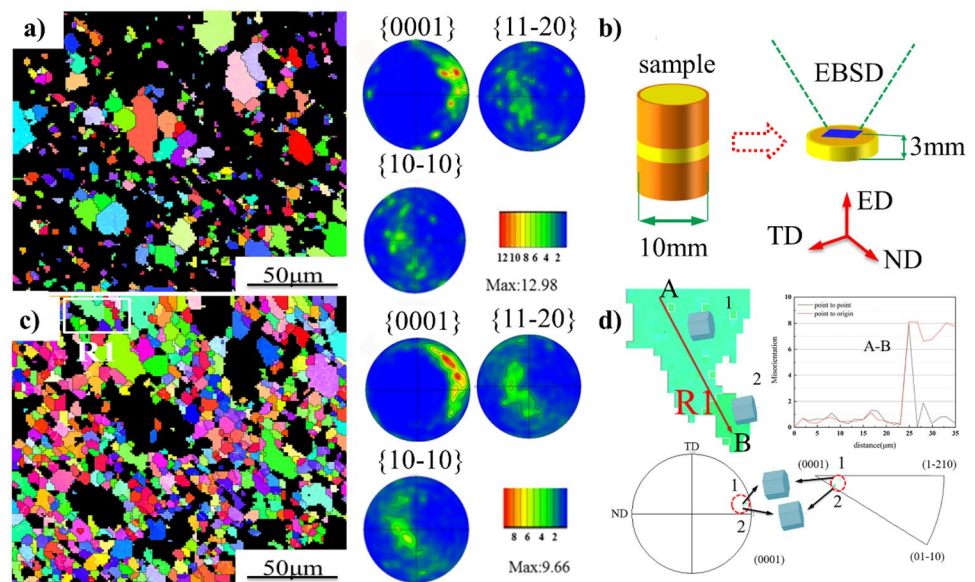
recrystallized grains are 38%. It is worth mentioning that subgrains make up a large percentage of the total, accounting for approximately 33%. In the process of alternating extrusion, the proportion of recrystallized and deformed grains is large, which leads to the formation of the maximum point of texture pole density. Although recrystallized grains make up a significant component of the pre-upsetting alternating extrusion process, the quantity of subgrains is also significant. Due to the accumulation of a large number of dislocations in the pre-upsetting alternate extrusion process to form subgrain boundaries, recrystallization has not yet been completed.

Figure 8 depicts the distribution of recrystallized and nonrecrystallized UAEF. The size of the recrystallized grains is generally larger, the texture strength formed by the recrystallized grains is higher, and the pole density can reach 12.98. The texture strength formed by the nonrecrystallized grain group is only 9.66, and the average grain size is also small. The texture strength of the recrystallized texture is significantly higher than that of the nonrecrystallized texture; therefore, it can be preliminarily judged that the recrystallized texture plays an important role in the formation of the pre-upsetting alternate extrusion texture. Select a typical area R1 (white rectangular frame) in Fig. 8b, which is a process of crushing and refining deformed grains. In the crushed and refined grains, dynamic recrystallization was not completed. In other words, grain boundary rotation and dislocation climbing did not promote the annihilation of high-density dislocations at the grain boundaries, so the grains were slacked to form recrystallized grains [41]. Therefore, these fine grains are identified as deformed grains in EBSD, and it can be

seen from Fig. 8d that there are some differences in grain orientation.

To further explore the formation of the texture of pre-upsetting alternating extrusion products, Fig. 9 is a pole figure comparison of the initial structure and the structure of the pre-upsetting. In Fig. 9a, it can be seen that the initial billet has a typical extruded fiber texture. In the process of alternating extrusion, many slip systems will be activated, and dislocations on different slip systems will also move synchronously [42]. Dislocation movement can promote grain rotation and activate the slip system in the easiest starting direction. The  $c$  axis of the base plane of most grains (0001) is parallel to the ND direction and perpendicular to the ED direction. Figure 9a is a schematic diagram of the grain orientation of the initial billet and after pre-upsetting, which shows that the initial texture already exists. After pre-upsetting, the preferred orientation of the grain base plane in the billet is weakened because in the pre-upsetting process, due to the obstruction of the edge, some grains in the billet rotate to a certain extent. The right pole figure also verifies that the texture strength decreases, and the maximum pole density of the pole figure is reduced from 21.25 to 17.06. After pre-upsetting, some grain base planes inclined in the ED direction, and a typical shear texture similar to that in ECAP was formed [43]. According to Fig. 9c, it can be preliminarily determined that it should be caused by some grain base planes parallel to the shear plane after pre-upsetting. On the other hand, it can be attributed to a discontinuous dynamic recrystallization mechanism [44]. To some extent, this particular texture will influence the texture generation of pre-upsetting alternate extrusion products.

**Fig. 8** Texture characteristics and comparison of the recrystallized grains and nonrecrystallized grains of AZ31 magnesium alloy under UAEF: **a**, **c** recrystallized grains and texture distribution; **b** schematic diagram of the location of electron backscatter diffraction (EBSD) measurement within the sample; **d** line profile of misorientation angle along AB





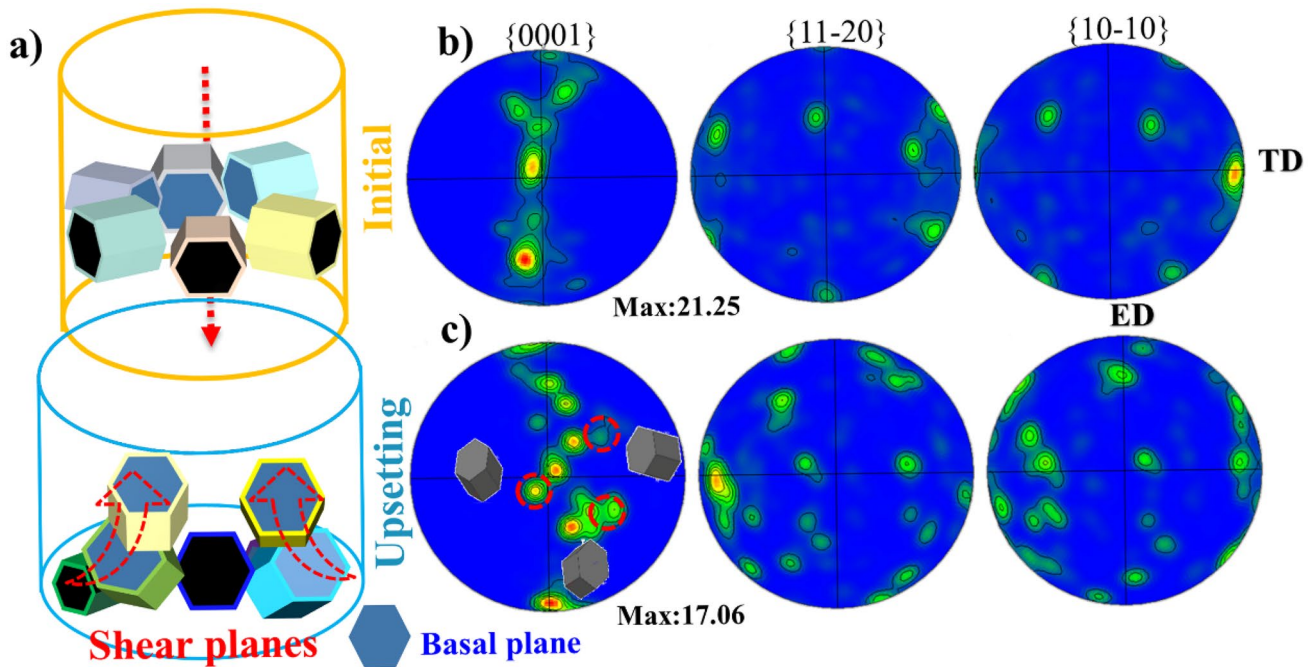


Fig. 9 Schematic diagrams of the texture evolution during upsetting. **a** Schematic diagram, **b** initial sample, and **c** upsetting sample

## 5 Conclusion

1. Research results show that UAFE can achieve a double increase in strength and ductility. Compared with interactive alternate forward extrusion, the tensile strength of the product of UAFE is increased from 198 to 281 MPa, and the ductility is increased from 12.5 to 23.7%.
2. The pre-upsetting process reduces the subsequent alternate extrusion load, and 159 kN of the conventional alternate extrusion is reduced to 115 kN. Increasing the Schmid factor in the initial sample, which reduced the single crystal yield strength during tensile testing, increased the resolved shear stress of the external force  $F$  on the slip, promoted the metal to easily start slipping, and caused plastic deformation.
3. Interactive alternate extrusion further refines the grains after pre-upsetting, and the average grain size is 5.65  $\mu\text{m}$ , which is only 1/2 of the average grain size of conventional alternating extrusion. According to Hall–Petch, fine-grained strengthening plays an important role in improving the yield strength of products, and the texture inclined to the ED direction is introduced during the pre-upsetting process, which effectively reduces the texture strength of subsequent alternating extrusion products, promotes nonbasal slip and improves the ductility of the material.

**Acknowledgements** This project is supported by the National Natural Science Foundation of China (No. 51975166).

**Author contribution** New extrusion technology is currently a hot research direction in the field of plastic processing. A predeformation alternating extrusion process was proposed in this paper, which can provide a new idea for the preparation of high-performance magnesium alloy.

**Availability of data and materials** The data obtained in the framework of this study are available to the journal upon request.

## Declarations

**Ethics approval** Not applicable.

**Consent to participate** Not applicable.

**Consent for publication** Not applicable.

**Competing interests** The authors declare no competing interests.

## References

1. Zeng ZR, Stanford N, Davies CHJ, Nie JF, Birbilis N (2019) Magnesium extrusion alloys: a review of developments and prospects. *Int Mater Rev* 64(1):27–62. <https://doi.org/10.1080/09506608.2017.1421439>

2. Song JF, She J, Chen DL, Pan FS (2020) Latest research advances on magnesium and magnesium alloys worldwide. *J Magnes Alloy* 8(1):1–41. <https://doi.org/10.1016/j.jma.2020.02.003>
3. Che B, Lu LW, Zhang JL, Zhang JH, Ma M, Wang LF, Qi FG (2022) Effects of cryogenic treatment on microstructure and mechanical properties of AZ31 magnesium alloy rolled at different paths. *Mater Sci Eng A* 832. <https://doi.org/10.1016/j.msea.2021.142475>
4. Zhang Z, Zhang JH, Xie JS, Liu SJ, He YY, Guan K, Wu RZ (2022) Developing a low-alloyed fine-grained Mg alloy with high strength-ductility based on dislocation evolution and grain boundary segregation. *Scr Mater* 209. <https://doi.org/10.1016/j.scriptamat.2021.114414>
5. Yan ZM, Li XB, Zheng J, Zhang ZM, Wang Q, Xu KH, Fan HZ, Zhang GS, Zhu JX, Xue Y (2021) Microstructure evolution, texture and mechanical properties of a Mg–Gd–Y–Zn–Zr alloy fabricated by cyclic expansion extrusion with an asymmetrical extrusion cavity: the influence of passes and processing route. *J Magnes Alloy* 9(3):964–982. <https://doi.org/10.1016/j.jma.2020.06.016>
6. Alaneme KK, Okotete EA (2017) Enhancing plastic deformability of Mg and its alloys—a review of traditional and nascent developments. *J Magnes Alloy* 5(4):460–475. <https://doi.org/10.1016/j.jma.2017.11.001>
7. Agnew SR, Nie JF (2010) Preface to the viewpoint set on: the current state of magnesium alloy science and technology. *Scr Mater* 63(7):671–673. <https://doi.org/10.1016/j.scriptamat.2010.06.029>
8. Pan FS, Wang QH, Jiang B, He JJ, Chai YF, Xu J (2016) An effective approach called the composite extrusion to improve the mechanical properties of AZ31 magnesium alloy sheets. *Mater Sci Eng A* 655:339–345. <https://doi.org/10.1016/j.msea.2015.12.098>
9. Lu LW, Liu CM, Zhao J, Zeng WB, Wang ZC (2015) Modification of grain refinement and texture in AZ31 Mg alloy by a new plastic deformation method. *J Alloys Compd* 628:130–134. <https://doi.org/10.1016/j.jallcom.2014.12.196>
10. Xu J, Song JF, Jiang B, He JJ, Wang QH, Liu B, Huang GS, Pan FS (2017) Effect of effective strain gradient on texture and mechanical properties of Mg-3Al-1Zn alloy sheets produced by asymmetric extrusion. *Mater Sci Eng A* 706:172–180. <https://doi.org/10.1016/j.msea.2017.09.004>
11. Li F, Zeng X, Chen Q, Cao GJ (2015) Effect of local strains on the texture and mechanical properties of AZ31 magnesium alloy produced by continuous variable cross-section direct extrusion (CVCDE). *Mater Des* 85:389–395. <https://doi.org/10.1016/j.matdes.2015.06.168>
12. Zhang WN, Zhang H, Wang LF, Fan JF, Li X, Zhu LL, Chen SY, Roven HJ, Zhang SZ (2020) Microstructure evolution and mechanical properties of AZ31 magnesium alloy sheets prepared by low-speed extrusion with different temperature. *Crystals* 10(8). <https://doi.org/10.3390/cryst10080644>
13. Wang Y, Li F, Wang Y, Gao L (2020) Effect of dynamic recrystallization on grain refinement during interactive alternating forward extrusion of AZ31B magnesium alloy. *J Mater Eng Perform* 29(5):2748–2756. <https://doi.org/10.1007/s11665-020-04780-3>
14. Wang Y, Li F, Wang Y, Xiao XM (2021) Texture property and weakening mechanism of Mg-3Al-1Zn alloy by interactive alternating forward extrusion. *J Magnes Alloy*. <https://doi.org/10.1016/j.jma.2021.05.007>
15. Li F, Jiang HW, Chen Q, Liu Y (2017) New extrusion method for reducing load and refining grains for magnesium alloy. *Int J Adv Manuf Technol* 90(1–4):73–79. <https://doi.org/10.1007/s00170-016-9323-8>
16. Li F, Jiang HW, Liu Y (2017) Microstructure and texture evolution during the alternate extrusion of an AZ31 magnesium alloy. *JOM* 69(1):93–99. <https://doi.org/10.1007/s11837-016-2146-0>
17. Al-Samman T, Gottstein G (2008) Room temperature formability of a magnesium AZ31 alloy: examining the role of texture on the deformation mechanisms. *Mater Sci Eng A* 488(1–2):406–414. <https://doi.org/10.1016/j.msea.2007.11.056>
18. Molodov KD, Al-Samman T, Molodov DA, Gottstein G (2014) Mechanisms of exceptional ductility of magnesium single crystal during deformation at room temperature: multiple twinning and dynamic recrystallization. *Acta Mater* 76:314–330. <https://doi.org/10.1016/j.actamat.2014.04.066>
19. Song B, Xin RL, Chen G, Zhang XY, Liu Q (2012) Improving tensile and compressive properties of magnesium alloy plates by pre-cold rolling. *Scr Mater* 66(12):1061–1064. <https://doi.org/10.1016/j.scriptamat.2012.02.047>
20. Zhang GS, Meng YZ, Yan FF, Gao Z, Yan ZM, Zhang ZM (2020) Microstructure and texture evolution of Mg-RE-Zn alloy prepared by repetitive upsetting-extrusion under different decreasing temperature degrees. *J Alloys Compd* 815. <https://doi.org/10.1016/j.jallcom.2019.152452>
21. Wang Y, Li F, Wang Y, Chen Q, Li XW, Fang WB (2022) Role of grain refinement mechanism on microstructure and performance in AZ31B alloy during interactive alternating forward extrusion (AFE) process. *Met Mater Int* 28(4):823–832. <https://doi.org/10.1007/s12540-020-00962-9>
22. Vaishakh KV, Narasimhan R, Yazar KU, Suwas S (2020) Mixed-mode (I and II) fracture behavior of a basal-textured magnesium alloy. *Acta Mater* 193:99–114. <https://doi.org/10.1016/j.actamat.2020.03.023>
23. Orlov D, Raab G, Lamark TT, Popov M, Estrin Y (2011) Improvement of mechanical properties of magnesium alloy ZK60 by integrated extrusion and equal channel angular pressing. *Acta Mater* 59(1):375–385. <https://doi.org/10.1016/j.actamat.2010.09.043>
24. Yan ZM, Zhang ZM, Li XB, Xu J, Wang Q, Zhang GS, Zheng J, Fan HZ, Xu KH, Zhu JX, Xue Y (2020) A novel severe plastic deformation method and its effect on microstructure, texture and mechanical properties of Mg-Gd-Y-Zn-Zr alloy. *J Alloys Compd* 822. <https://doi.org/10.1016/j.jallcom.2020.153698>
25. Yuan W, Panigrahi SK, Su JQ, Mishra RS (2011) Influence of grain size and texture on Hall-Petch relationship for a magnesium alloy. *Scr Mater* 65(11):994–997. <https://doi.org/10.1016/j.scriptamat.2011.08.028>
26. Li CL, Mei QS, Li JY, Chen F, Ma Y, Mei XM (2018) Hall-Petch relations and strengthening of Al-ZnO composites in view of grain size relative to interparticle spacing. *Scr Mater* 153:27–30. <https://doi.org/10.1016/j.scriptamat.2018.04.042>
27. Hansen N (2004) Hall-Petch relation and boundary strengthening. *Scr Mater* 51(8):801–806. <https://doi.org/10.1016/j.scriptamat.2004.06.002>
28. Wang C, Ning H, Liu S, You J, Wang T, Jia HJ, Zha M, Wang HY (2021) Enhanced ductility and strength of Mg-1Zn-1Sn-0.3Y-0.2Ca alloy achieved by novel micro-texture design. *Scr Mater* 204. <https://doi.org/10.1016/j.scriptamat.2021.114119>
29. Xu J, Yang TH, Jiang B, Song JF, He JJ, Wang Q, Chai YF, Huang GS, Pan FS (2018) Improved mechanical properties of Mg-3Al-1Zn alloy sheets by optimizing the extrusion die angles: microstructural and texture evolution. *J Alloys Compd* 762:719–729. <https://doi.org/10.1016/j.jallcom.2018.05.083>
30. Srinivasarao B, Dudamell NV, Perez-Prado MT (2013) Texture analysis of the effect of non-basal slip systems on the dynamic recrystallization of the Mg alloy AZ31. *Mater Charact* 75:101–107. <https://doi.org/10.1016/j.matchar.2012.10.002>
31. Koike J, Ohyama R (2005) Geometrical c-Tierion for the activation of prismatic slip in AZ61 Mg alloy sheets deformed at room temperature. *Acta Mater* 53(7):1963–1972. <https://doi.org/10.1016/j.actamat.2005.01.008>
32. Nan XL, Wang HY, Zhang L, Li JB, Jiang QC (2012) Calculation of Schmid factors in magnesium: analysis of deformation

- behaviors. *Scr Mater* 67(5):443–446. <https://doi.org/10.1016/j.scriptamat.2012.05.042>
33. Qin DH, Wang MJ, Sun CY, Su ZX, Qian LY, Sun ZH (2020) Interaction between texture evolution and dynamic recrystallization of extruded AZ80 magnesium alloy during hot deformation. *Mater Sci Eng A* 788. <https://doi.org/10.1016/j.msea.2020.139537>
34. Gui YW, Ouyang LX, Cui YJ, Bian HK, Li QA, Chiba A (2021) Grain refinement and weak-textured structures based on the dynamic recrystallization of Mg-9.80Gd-3.78Y-1.12Sm-0.48Zr alloy. *J Magnes Alloy* 9(2):456–466. <https://doi.org/10.1016/j.jma.2020.06.001>
35. Cepeda-Jimenez CM, Molina-Aldareguia JM, Perez-Prado MT (2015) Origin of the twinning to slip transition with grain size refinement, with decreasing strain rate and with increasing temperature in magnesium. *Acta Mater* 88:232–244. <https://doi.org/10.1016/j.actamat.2015.01.032>
36. Jiang MG, Xu C, Yan H, Fan GH, Nakata T, Lao CS, Chen RS, Kamado S, Han EH, Lu BH (2018) Unveiling the formation of basal texture variations based on twinning and dynamic recrystallization in AZ31 magnesium alloy during extrusion. *Acta Mater* 157:53–71. <https://doi.org/10.1016/j.actamat.2018.07.014>
37. Tong LB, Chu JH, Sun WT, Jiang ZH, Zou DN, Liu SF, Kamado S, Zheng MY (2021) Development of a high-strength Mg alloy with superior ductility through a unique texture modification from equal channel angular pressing. *J Magnes Alloy* 9(3):1007–1018. <https://doi.org/10.1016/j.jma.2020.03.011>
38. Wang Y, Chen G, Chen Z, Wan H, Xiao H, Chang X (2022) Electropulsing assisted aging with ultrafast hardening rate for AerMet100 steel. *Mater Sci Eng A* 841:143066. <https://doi.org/10.1016/j.msea.2022.143066>
39. Gehrman R, Frommert MM, Gottstein G (2005) Texture effects on plastic deformation of magnesium. *Mater Sci Eng A* 395(1–2):338–349. <https://doi.org/10.1016/j.msea.2005.01.002>
40. Wu XL, Zhu YT (2017) Heterogeneous materials: a new class of materials with unprecedented mechanical properties. *Mater Res Lett* 5(8):527–532. <https://doi.org/10.1080/21663831.2017.1343208>
41. Sandlobes S, Friak M, Zaefferer S, Dick A, Yi S, Letzig D, Pei Z, Zhu LF, Neugebauer J, Raabe D (2012) The relation between ductility and stacking fault energies in Mg and Mg-Y alloys. *Acta Mater* 60(6–7):3011–3021. <https://doi.org/10.1016/j.actamat.2012.02.006>
42. Hou DW, Liu TM, Chen HC, Shi DF, Ran CH, Pan FS (2016) Analysis of the microstructure and deformation mechanisms by compression along normal direction in a rolled AZ31 magnesium alloy. *Mater Sci Eng A* 660:102–107. <https://doi.org/10.1016/j.msea.2016.02.020>
43. Foley DC, Al-Maharbi M, Hartwig KT, Karaman I, Kecskes LJ, Mathaudhu SN (2011) Grain refinement vs. crystallographic texture: mechanical anisotropy in a magnesium alloy. *Scr Mater* 64(2):193–196. <https://doi.org/10.1016/j.scriptamat.2010.09.042>
44. Liu W, Ma YB, Zhang YG, Fan XX, Xu CX, Zhang JS (2017) Two dynamic recrystallization processes in a high-performance extruded Mg94.5Y2Gd1Zn2Mn0.5 alloy. *Mater Sci Eng A* 690:132–136. <https://doi.org/10.1016/j.msea.2017.02.088>

**Publisher's Note** Springer Nature remains neutral with regard to jurisdictional claims in published maps and institutional affiliations.